ACS APPLIED MATERIALS & INTERFACES

Research Article

Cite This: ACS Appl. Mater. Interfaces XXXX, XXX, XXX−XXX

www.acsami.org

Toward High Areal Energy and Power Density Electrode for Li-Ion Batteries via Optimized 3D Printing Approach

Jiwei Wang,[†,‡,§] Qian Sun,[‡] Xuejie Gao,[‡,§] Changhong Wang,[‡] Weihan Li,[‡,§] Frederick Benjamin Holness,[‡] Matthew Zheng,[‡] Ruying Li,[‡] Aaron David Price,[‡] Xuhui Sun,[*,†] Tsun-Kong Sham,[*,§] and Xueliang Sun[*,‡]

[†]Soochow University-Western University Center for Synchrotron Radiation Research, Institute of Functional Nano and Soft Materials (FUNSOM), Jiangsu Key Laboratory for Carbon-Based Functional Materials & Devices, Soochow University, Suzhou 215123, China

[‡]Department of Mechanical and Materials Engineering, University of Western Ontario, London, Ontario N6A 5B9, Canada

[§]Department of Chemistry, University of Western Ontario, London, Ontario N6A 5B7, Canada

Supporting Information

ABSTRACT: High-energy and high-power-density lithium-ion batteries are promising energy storage systems for future portable electronics and electric vehicles. Here, three-dimensional (3D) patterned electrodes are created through the paste-extrusion-based 3D printing technique realizing a trade-off between high energy density and power density. The 3D electrodes possess several distinct merits over traditional flat thick electrodes, such as higher surface area, shorter ion transport path, and improved mechanical strength. Benefiting from these advantages, the 3D-printed thick electrodes present the higher specific capacity and improved cycling stability compared with those of the conventional thick electrodes. Upon comparison to the previous studies on 3D-printed electrodes, this study investigates the influence and optimization of 3D-printed $LiFePO_4$ (LFP) electrodes with three different geometric shapes to achieve a high rate performance and long-term cycling stability. Accordingly, a series of 3D electrodes with different thickness were created, and an ultrathick (1500 μm) 3D-patterned electrode exhibits a high areal capacity of around 7.5 mA h cm^{-2}, presenting remarkable value for state-of-the-art LFP cathodes. This work demonstrates patternable 3D printing as a potential strategy to fabricate thick electrodes toward high areal energy density and power density, which holds great promise for the future development of high-performance energy storage devices.

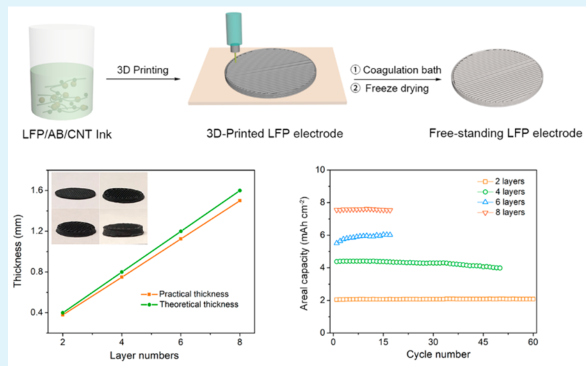

KEYWORDS: *high areal energy and power density, paste extrusion, three-dimensional (3D) printing technique, 3D-patterned thick $LiFePO_4$ (LFP) electrodes, patternable 3D printing*

1. INTRODUCTION

The advance of portable electronics and electric vehicles has stimulated the development of energy storage devices with increasingly higher energy density and power density during the past decades.[1−4] To meet the growing demands for advanced energy storage systems, tremendous efforts have been devoted to developing new electrode materials with high capacity.[5−7] The design of electrode architectures for achieving higher-energy-density and higher-power-density storage devices is a particular point of focus. Regarding this respect, it is important to have the capability to optimize the electrode architecture design as it greatly affects the transport of ions and electrons, as well as the kinetic reaction.[8−12] One promising strategy is to create thicker electrodes with higher areal mass loading to meet the high-energy-density requirement.[13] Unfortunately, the traditional blade-cast thick electrode limits the transport of ions and electrons across the thick electrode, resulting in poor power density and incomplete utilization of active materials.[8,14] Moreover, the active material detaches from the current collector with cycling, leading to a shorter cycle life. Three-dimensional (3D) batteries have been proposed to be a promising alternative approach to achieve a trade-off between high energy density and power density.[15] Batteries with 3D architectures can possess higher energy density by increasing the electrode height to provide more active materials, while the ion diffusion length could be maintained at a constant value, suggesting that the energy density can be improved without sacrificing power density.

Three-dimensional printing, also known as advanced additive manufacturing (AM), has recently attracted much

Received: August 27, 2018
Accepted: October 29, 2018
Published: October 29, 2018

DOI: 10.1021/acsami.8b14797
ACS Appl. Mater. Interfaces XXXX, XXX, XXX−XXX

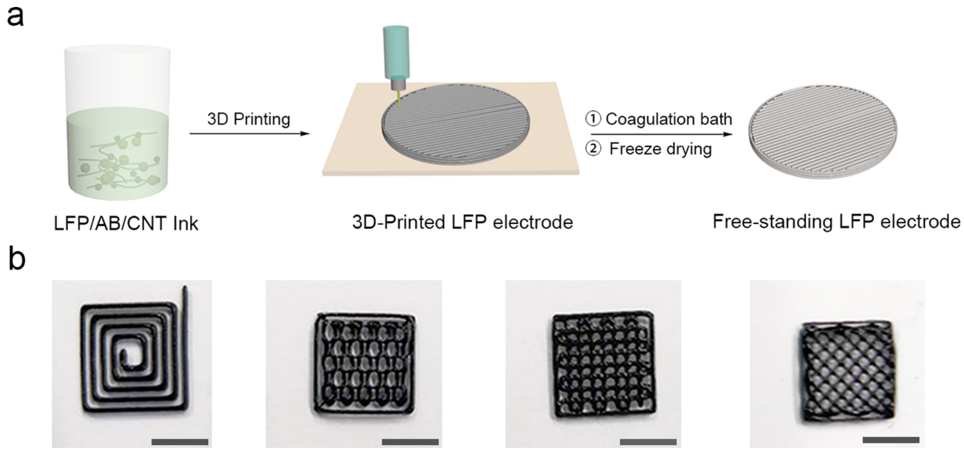

Figure 1. (a) Schematic illustration of 3D-printed self-supported LFP electrodes. (b) Optical images of 3D-printed LFP structure with various patterns (scale bars: 7 mm).

attention in the energy storage field due to its capability to enable the construction of complex 3D architectures accurately and efficiently.[16−20] Importantly, 3D printing techniques can control electrode thickness by simply adjusting the printing layer count, changing the printing nozzle, and modifying the printing speed and pressures.[21−23] For instance, Lewis and co-workers fabricated the first 3D-printed interdigitated Li-ion microbattery architectures using a paste-extrusion-type printing technique, where the printable cathode and anode inks were composed of $LiFePO_4$ (LFP) and $Li_4Ti_5O_{12}$ (LTO) nanoparticles dispersed in a highly concentrated slurry.[24] Later on, Hu and co-workers successfully fabricated an interdigitated Li-ion microbattery via a 3D printing technique based on graphene oxide (GO) composite inks consisting of highly concentrated GO suspensions with the cathode (LFP) and anode (LTO) active materials added.[25] The printed full cell displayed a relatively stable discharge capacity of 91 mA h g^{-1}, corresponding to a high areal capacity of 1.64 mA h cm^{-2} based on the high electrode mass loading of around 18 mg cm^{-2}. More recently, the 3D-printed hierarchical porous framework containing graphene/$Na_3V_2(PO_4)_3$ composite as Na-ion battery cathode was reported and displayed a high specific capacity as well as better cycling stability up to 900 cycles.[26] Despite the progress being made on 3D printing for batteries, there has yet been a study that investigates the electrode micropattern effects on the electrochemical performance through the 3D printing technique. Meanwhile, great challenges still lie in the pursuit to develop low-cost, facile, and scalable printing processes/inks for practical application in future advanced energy storage systems.

Herein, for the first time, we report the design of various 3D-patterned thick LFP electrodes that achieved high areal energy density performance through an optimized extrusion-based 3D printing approach. The printing ink in this work is quite similar to the general electrode slurry composition used for lithium-ion batteries, which consists of LFP nanoparticles active material, acetylene black (AB), and multiwalled carbon nanotubes (MWCNTs) dispersed in a highly concentrated slurry composed of poly(vinylidene fluoride-*co*-hexafluoropropylene) (PVDF-HFP) dissolved in N-methyl-2-pyrrolidone (NMP). The 3D-printed microstructured electrodes showed several distinct advantages over the conventional slurry-coated thick electrode: (1) The well-designed macropores in 3D-patterned architectures could increase the surface area of the electrode and facilitate the penetration of electrolyte into the active materials. (2) The continuous filaments composed of interconnected porous polymer framework and conducting MWCNT networks with controllable interdistance are able to accelerate the electron and ion transport. Moreover, the 3D-patterned thick electrode is composed of the filament with a shorter lithium-ion diffusion length (less than 150 μm) than that of the conventional slurry coating thick electrode. (3) The mechanical strength of the 3D-printed structures could help mitigate the challenge of deformation in conventional thick electrodes, thus improving the cycling stability of lithium-ion batteries (LIBs) under high loading. As a result, three types of 3D-printed patterned thick electrodes have been developed; each of them presents a higher specific capacity and improved cycling stability compared with those of the conventional flat thick electrode. Furthermore, we fabricated a series of 3D electrodes with different printing layers and an ultrathick (1500 μm) 8-layer 3D-patterned electrode with an areal mass loading of around 50 mg cm^{-2}, exhibiting the high areal capacity of around 7.5 mA h cm^{-2} and presenting a desirable value for LFP cathode in practical high-energy-density LIBs applications.

2. EXPERIMENTAL SECTION

Preparation of LFP Ink. Commercialized LFP nanoparticles were used as the active materials. Highly concentrated LFP ink was prepared by first mixing 1400 mg of LFP nanoparticles, 200 mg of acetylene black (AB), and 100 mg of multiwall carbon nanotubes (MWCNTs, diameter of 40−60 nm, length of 2 μm) and grinding them well for a few minutes. Then 300 mg of PVDF-HFP powder (M_w ∼ 400 000, Sigma-Aldrich) was dissolved in 1200 mg of 1-methyl-2-pyrrolidinone (NMP, Sigma-Aldrich), which was added into the mixed powder as a binder. Afterward, the obtained concentrated LFP gel was further mixed in a conditioning mixer (ARM 310, Thinky) at 2000 rpm for 25 min. Finally, a homogenized LFP paste was obtained for the 3D printing process.

3D Printing Process. The as-prepared LFP ink was used to fabricate 3D-structured electrodes by using a fused filament fabrication (FFF) DeltaMaker 3D printer modified with a paste-extrusion-type tool head. In detail, the as-prepared LFP ink was first loaded into a 3 cm^3 syringe. The syringe was subsequently subject to centrifugation at 3000 rpm for 3 min to expel out all air bubbles in the ink. A metal nozzle with an inner diameter of 200 μm was adopted, and a Nordson EFD computer-controlled pneumatic fluid dispenser was used to control the printing extrusion pressures between 30 and 50 psi. The printing speed ranges from 6 to 10 mm s^{-1}. After printing,

DOI: 10.1021/acsami.8b14797
ACS Appl. Mater. Interfaces XXXX, XXX, XXX−XXX

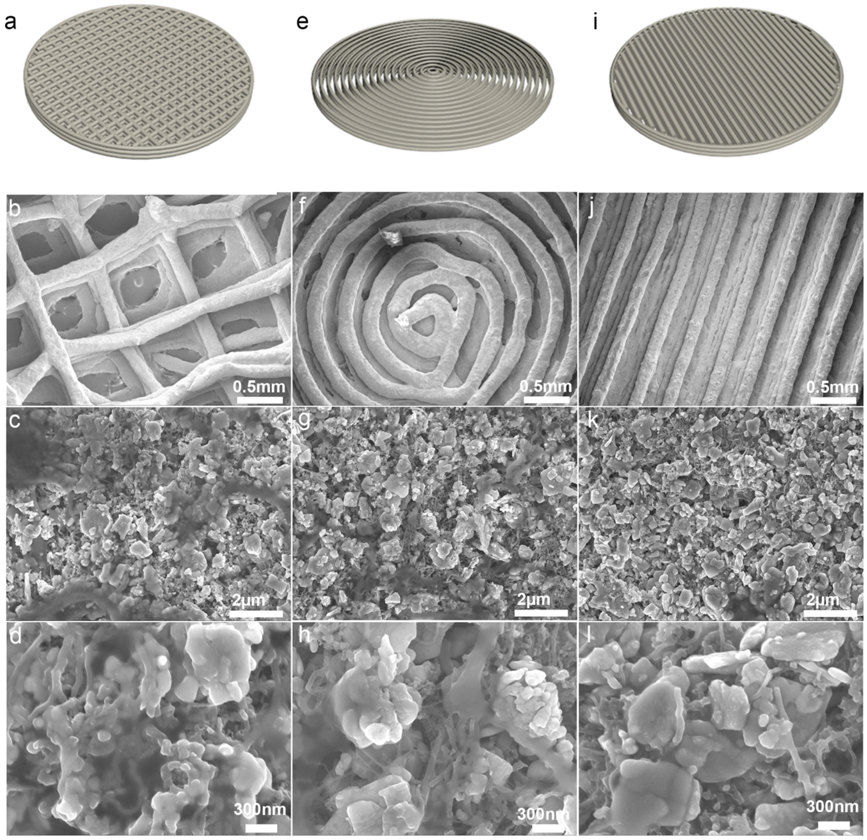

Figure 2. Schematic and SEM images of three types of 3D-printed LFP electrodes. (a) Schematic illustration and (b−d) SEM images of a 3D-printed circle-grid pattern LFP electrode. (e) Schematic illustration and (f−h) SEM images of a 3D-printed circle-ring pattern LFP electrode. (i) Schematic illustration and (j−l) SEM images of a 3D-printed circle-line pattern LFP electrode.

the 3D structures were first immersed into a water coagulation bath for few minutes to remove the solvent, followed by freeze-drying for 24 h.

Materials Characterizations. The morphologies of all the samples were observed by using a Hitachi S-4800 field-emission scanning electron microscope (SEM). X-ray diffraction (XRD) measurements were conducted using a Bruker D8 Advance (Cu Kα source, 40 kV, 40 mA) spectrometer.

Electrochemical Measurements. The electrochemical performances of the 3D-printed LFP electrodes were tested in 2032-coin-cells. All cells were assembled in an Ar-filled glovebox with Li foil as counter and reference electrodes. The liquid electrolyte was 1 M $LiPF_6$ dissolved in a mixture of ethylene carbonate (EC), dimethyl carbonate (DMC), and diethyl carbonate (DEC) with a volume ratio of 1:1:1. The galvanostatic charge−discharge performance was evaluated with a LAND test system in the voltage range 2.5−4.2 V (vs Li^+/Li) at room temperature.

3. RESULTS AND DISCUSSION

Figure 1a is a schematic illustration of the fabrication process of 3D printing self-supported LFP electrodes. The printable LFP composite ink (Figure S1a) was prepared by first adding LFP nanoparticles, AB, and MWCNTs into PVDF-HFP/NMP to form the slurry. The high-concentration mixture was then mixed homogeneously by a Thinky mixer prior to the printing process. Subsequently, the obtained LFP ink was loaded into a syringe as shown in Figure S1b and then extruded through a metal nozzle with an inner diameter of 200 μm onto a glass slice substrate. The process was controlled by a predesigned program. The 3D-printed object together with the glass slice substrate were then subjected to a water bath for solvent exchange. After soaking in the water bath for a few minutes, the printed structure was smoothly peeled off from the glass substrate, and a free-standing electrode with a smooth surface and improved mechanical strength was obtained after freeze-drying for 24 h. Figure 1b shows various 3D-printed complex shapes and structures designed by 3D-software, demonstrating that the 3D printing technique has great ability and potential in fabricating batteries with complex shapes and configurations.

Since 3D printing can construct various shapes and structures, three typical circle-shaped patterns were selected for printing LFP electrodes to explore the best electrochemical performance in coin-cell LIBs as shown in Figure S2. The microstructures and morphologies of the three types of 3D-printed LFP electrodes were first investigated by scanning electron microscopy (SEM) as shown in Figure 2. Figure 2a,e,i shows the schematic of the circle-grid, circle-ring, and circle-line pattern LFP electrodes, respectively. The microstructure of the gridlike pattern is clearly visible in Figure 2b. The diameter of the filament is around 100−150 μm, which is a little smaller than that of the metal nozzle used for the printing. The diameter decreasing results from the shrinkage of the polymer binder during the solvent removal step in the drying processes. It should be noted that the decreased diameter of the dried filament might reduce the ion transport length, thereby improving the rate performance of the electrodes. The interval between the two filaments, which could be controlled by the printing procedure, is controlled to be around 500 μm. The well-designed interval space was able to facilitate the diffusion of electrolyte to the active materials. The surface of the filament is very smooth, and each filament shows a very dense

DOI: 10.1021/acsami.8b14797
ACS Appl. Mater. Interfaces XXXX, XXX, XXX−XXX

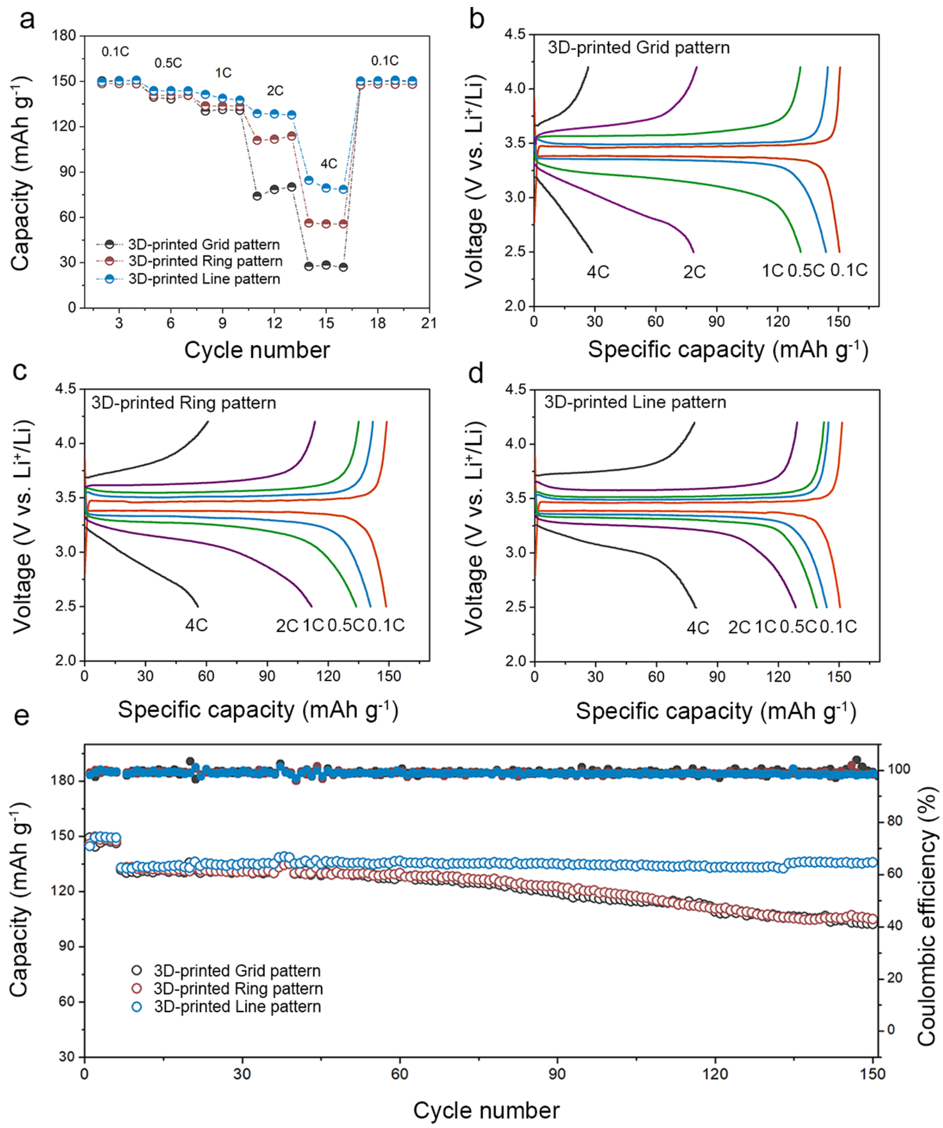

Figure 3. Electrochemical performance of the three types of 3D-printed LFP electrodes. (a) Comparison of rate performance of the three types of LFP electrodes. Charge−discharge voltage curves of (b) the 3D-printed grid pattern, (c) the 3D-printed ring pattern, and (d) the 3D-printed line pattern LFP electrodes at various rates. (e) Cycling performance of the three types of LFP electrodes at 1 C with the first six cycles activated at 0.1 C.

structure, ensuring a high material loading density. The magnified SEM images in Figure 2c,d show that the LFP nanoparticles and AB nanoparticles are uniformly wrapped by the PVDF-HFP binder, and the CNTs are interconnected between the LFP and AB nanoparticles, thus forming an interconnected porous framework and continuous conducting network. Figure 2f,j shows the microstructure with a ringlike pattern and linelike pattern, respectively. The diameters of the filaments in these two patterns are similar to that of the grid pattern. The magnified SEM images in Figure 2h,i also reveal that these two patterned electrodes are constructed by the layered filaments consisting of the active material wrapped by a porous polymer framework and conducting carbon network, thereby facilitating the ion/electron transport.

To further examine the uniform distribution of LFP nanoparticles into the printed architectures, SEM-EDS elemental mapping was carried out as shown in Figure S3. The elemental mapping images suggest a homogeneous distribution of C, F, Fe, P, and O in the whole structure. Figure S4 shows the EDS spectra and corresponding elemental percentage table of the 3D-printed LFP electrode. The atomic ratio of Fe:P:O in the printed electrode is around 0.94:1:4.3, which is very close to the theoretical atomic ratio of Fe:P:O (1:1:4). To verify the phase stability of the LFP during the ink preparation and freeze-drying process, an X-ray diffraction (XRD) measurement was conducted to compare the phase of pristine LFP nanoparticles and that of the 3D-printed LFP electrodes. As presented in Figure S5, the LFP powders and 3D-printed LFP electrodes exhibit the same diffraction peaks, indicating that the ink preparation and postdrying process did not alter the crystal phase of the LFP, which is critical for maintaining desired electrochemical performance.

The electrochemical performances of the three types of 3D-printed LFP electrodes were evaluated in coin-cells. All three LFP electrodes have an areal mass loading of around 10 mg cm^{-2}. The rate capabilities of the three types of 3D-printed LFP electrodes were first examined at different rates from 0.1 to 4.0 C within the voltage window 2.5−4.2 V. As shown in

DOI: 10.1021/acsami.8b14797
ACS Appl. Mater. Interfaces XXXX, XXX, XXX−XXX

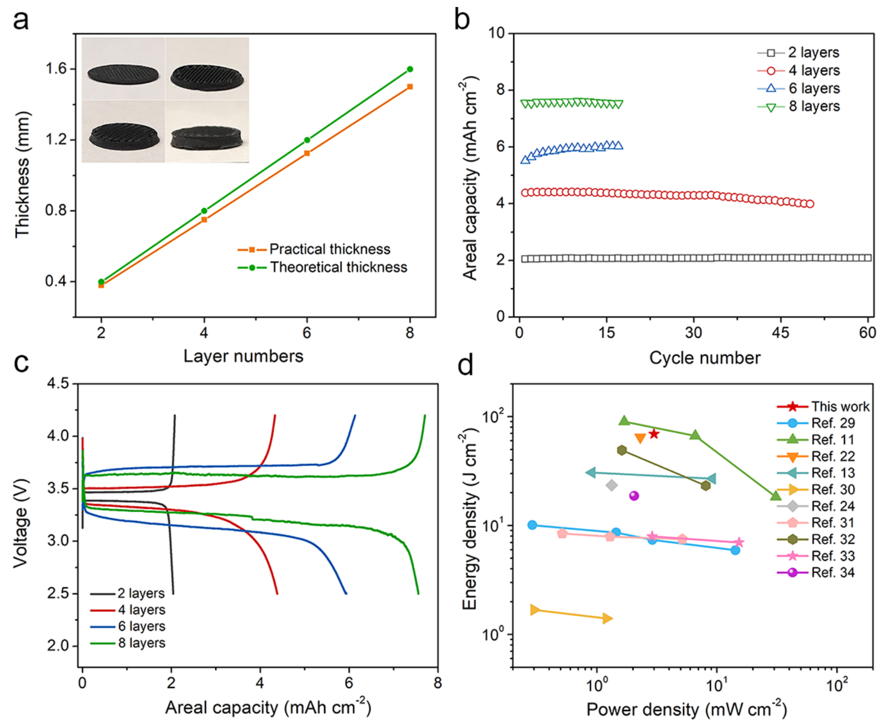

Figure 4. (a) Practical and theoretical thickness of the 3D-printed electrodes as a function of the printing layer number (inset: optical images of 3D-printed electrodes with different printing layers). (b) Comparison of the areal capacity of the LFP electrodes with different layer numbers. (c) Charge−discharge profiles of the LFP electrodes with different layer numbers. (d) Comparison of power density and energy density of this work with previously reported values.

Figure 3a, each of the three types of LFP electrodes exhibits the high specific capacity of around 150 mA h g^{-1} at a low current density of 0.1 C at the initial cycle, close to the theoretical specific capacity of LFP (170 mA h g^{-1}). It is interesting that the three types of LFP electrodes present similar specific capacities when cycling at lower C-rates such as 0.1, 0.5, and 1 C; however, the specific capacities show obvious differences at higher C-rates of 2.0 and 4.0 C among the three patterned LFP electrodes. When the current density changed back to 0.1 C, all of the three patterned LFP electrodes exhibit a specific capacity of around 150 mA h g^{-1}, indicating a good reversibility of the 3D-printed LFP electrode. The rate performance comparison among the three patterned LFP electrodes indicates that the microstructures of the electrodes have a distinct effect on the battery performance. Figure 3b−d shows the charge−discharge curves of the three patterned electrodes at various current densities, revealing a clear pattern on the electrochemical behavior of the cells. The comparison of overpotential at various current densities for the three types of patterned electrodes is presented in Figure S6. It should be noted that the line-patterned electrode exhibits much lower overpotential at various cycling rates due to its well-designed microstructure, facilitating the ion and electron transport, particularly at high current densities.

The cycling stability of the 3D-printed patterned LFP electrodes was further examined at the current density of 1 C with the first six cycles activated at 0.1 C. As shown in Figure 3e, the initial discharge capacities of the grid-, ring-, and line-patterned electrodes are 149.3, 145.8, and 144.6 mA h g^{-1}, with the initial Coulombic efficiency of 98.88%, 98.98%, and 98.14%, respectively. Each of the three patterned LFP electrodes displayed the discharge capacity of around 132 mA h g^{-1} after a few cycles at the lower current density of 0.1 C. Moreover, the line-patterned electrode presents an excellent cyclability over 150 cycles without any capacity fading. By contrast, the grid-patterned and ring-patterned electrodes deliver a discharge capacity of 102.4 and 105 mA h g^{-1}, demonstrating the capacity retention of 77.4% and 79.1%, respectively. This result suggests that the line-pattern microstructure possesses more advantages over the other two patterned microstructures, which is in accordance with the results from the rate performance comparison. For demonstrating the advantages of 3D-printed electrodes in achieving high-performance batteries, conventional slurry-coated thick electrodes were fabricated to compare with 3D-patterned electrodes. As observed in Figure S7a, the electrode with an areal mass loading of around 10 mg cm^{-2} was prepared by using the slurry with the same composition with the printing ink. Some cracks were observed on the electrode. When the thickness of the conventional electrode was further increased, as demonstrated in Figure S7b, severe electrode cracking and detachment from the Al current collector was observed. This phenomenon is common in thick electrodes fabricated by a typical slurry coating process, and can be attributed to the weak adhesion between the electrode components and metal current collectors and the shrinkage of the electrode materials during the drying process, which causes a failure to maintain the electrode structural integrity.[11,27,28] The ease of deformation of the conventional thick electrode leads to the shorter cycle life and poor safety. As shown in Figure S7c, the conventional thick electrode with an areal mass loading of around 10 mg cm^{-2} exhibits an initial discharge capacity of approximately 124 mA h g^{-1} with a dramatic capacity fade occurring with a capacity retention of 51.8% after 115 cycles. This comparison clearly indicates that all the 3D-printed patterned electrodes show an improved specific capacity and

DOI: 10.1021/acsami.8b14797
ACS Appl. Mater. Interfaces XXXX, XXX, XXX−XXX

cycling stability compared to the performance of the conventional thick electrode. The enhanced electrochemical performance of 3D-printed electrodes can be ascribed to the microscaled and nanoscaled multichanneled architecture, which allows for fast lithium-ion diffusion and efficient electrolyte penetration. In addition, the superior mechanical structure stability of the 3D-printed patterned electrodes is also a factor that contributes to the enhanced cycling stability.

To further consider the superiorities of the 3D printing technique in building high-performance thick electrodes for LIBs, a series of line-patterned LFP electrodes with different thickness were fabricated by the 3D printing method. Figure S8 shows four 3D-patterned electrodes with different printing layers (2 layers, 4 layers, 6 layers, and 8 layers) on a same glass slice substrate before drying. After coagulation in a water bath followed by freeze-drying, free-standing electrodes with increased mechanical strength were obtained, and the predesigned patterned structures were successfully reproduced (inset in Figure 4a). Figure 4a presents the comparison of the practical and theoretical thickness of the printed electrodes as a function of the printing layer number. The theoretical thickness of one layer is set to be 0.2 mm. It should be noted that the practical value of the electrode's thickness is a little bit smaller than the theoretical value due to above-mentioned shrinking. As shown in Figure S9, the thickness of 8 layers of electrode is 1.5 mm, and the printed electrode thickness demonstrates an approximately linear relationship with the printing layer number, which can be ascribed to the uniform features of each printing filament layer. This result also discloses that the bottom filament layer is mechanically strong enough to maintain the structure during the entire layer-by-layer printing process.

The electrochemical performance comparison of the 3D-printed electrodes with different printing layers is displayed in Figure 4b. It clearly shows that electrodes with 2 layers, 4 layers, 6 layers, and 8 layers exhibit the high stable areal capacity of around 2.07, 4.3, 6.0, and 7.5 mA h cm^{-2}, respectively. All these areal capacity values, especially 7.5 mA h cm^{-2}, demonstrate the practical application for LFP cathodes in LIBs. Moreover, it should be mentioned that the areal capacity values of different layered electrodes reveal an almost linear relationship with the layer number except for the 8-layered electrode. This phenomenon further confirms that the 3D structure is beneficial for ion transportation even within an ultrathick electrode. Figure 4c shows the charge−discharge profiles of the 3D-printed LFP electrodes with different layers, all presenting typical charge−discharge plateaus at around 3.5 V. The plotted curve in Figure 4d clearly displays the comparison of this work with previously reported data in the literature, in terms of areal energy and power densities.[11,13,22,24,29−34] As highlighted with a red star, the 3D-printed 8-layered line-patterned electrode could present the high areal energy density of 69.41 J cm^{-2} at the power density of 2.99 mW cm^{-2}, thereby demonstrating great potential for practical high-energy-density LIBs applications. The superior performance can be ascribed to a well-designed 3D architecture that possesses short transport length which facilitates ion and electron diffusion during the cycling process, as well as accommodating substantial amounts of active materials which realizes high areal capacity.

Three-dimensional electrodes with well-designed architectures via the 3D printing technique have been proven to show many advantages over conventional slurry-coated flat electrodes in terms of delivering enhanced areal energy density, better power density, and cycling stability. As illustrated in Figure 5,

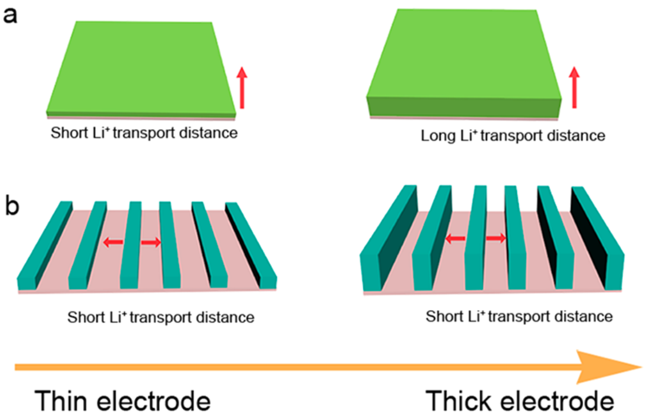

Figure 5. Schematic illustration of the comparison between ultrathick (a) traditional electrodes and (b) 3D electrodes.

although high power density can be achieved with a short ion transport distance, conventional thin electrodes can only deliver the low energy density as it lacks active materials. When a thick electrode is constructed by the conventional slurry coating method, the high energy density could be realized; however, the power density would be greatly restricted as the ion transport distance increases substantially. To this end, 3D electrodes can realize a trade-off between the high energy density and power density by maintaining a short and uniform ion diffusion path, ensuring that the thick electrode can achieve high power density. Compared to previous 3D-printed LFP, this work demonstrates greatly improved power and energy density due to the optimized 3D printing process as well as the geometric considerations. This work also demonstrates that 3D-printed electrodes can realize the highest level of areal loading as compared to other advanced 3D electrode manufacturing methods.

4. CONCLUSION

Three-dimensionally patterned self-supported thick electrodes for high-areal-energy and high-power-density LIBs have been realized by an optimized extrusion-type 3D printing technique. The resulting unique 3D-structured electrodes were constructed by continuous layer-by-layer filaments composed of interconnected porous polymer frameworks and continuous conducting carbon networks, thereby greatly improving ion and electron transport. The well-designed 3D microstructures were demonstrated to increase the surface area and maintain a short ion transport distance even within a thick electrode, facilitating the electrolyte penetration into the active materials as well as ion/electron diffusion. Due to these structural merits, the 3D-patterned electrodes exhibited superior electrochemical performance over conventional thick flat electrodes in terms of specific capacity and cycling stability. Moreover, an ultrathick electrode of 1500 μm 3D electrodes with 8 printed layers was fabricated and presented a high areal capacity of approximately 7.5 mA h cm^{-2} and energy density of 69.41 J cm^{-2} at a power density of 2.99 mW cm^{-2}, demonstrating comparable values with reported high-performance LFP cathodes fabricated by both 3D printing and other methods in the literature. This work thus provides a facile, low-cost, and easily scaled way to fabricate a high areal loading/thick electrode to achieve high

DOI: 10.1021/acsami.8b14797
ACS Appl. Mater. Interfaces XXXX, XXX, XXX−XXX

areal energy density with high power density, which holds great promise for future practical applications of high-energy-density lithium-ion batteries.

ASSOCIATED CONTENT

Supporting Information

The Supporting Information is available free of charge on the ACS Publications website at DOI: 10.1021/acsami.8b14797.

Optical images of the LFP ink and the 3D-printed three patterns of the LFP electrodes, SEM images and corresponding mapping of the printed LFP electrode, XRD of the LFP electrode, conventional cast LFP electrodes and cycling performance, photos of printed LFP with different layers, thickness of printed 8 layers LFP electrodes (PDF)

AUTHOR INFORMATION

Corresponding Authors

*E-mail: xhsun@suda.edu.cn.
*E-mail: tsham@uwo.ca.
*E-mail: xsun@eng.uwo.ca.

ORCID

Qian Sun: 0000-0001-5399-1440
Xuhui Sun: 0000-0003-0002-1146
Xueliang Sun: 0000-0003-2881-8237

Author Contributions

Xuhui Sun, Tsun-Kong Sham, and Xueliang Sun directed the project. Jiwei Wang conceived the idea, designed the experiments, and wrote the manuscript. Qian Sun gave some suggestions for the experiments and manuscript. Xuejie Gao helped with the freeze-drying. Weihan Li and Changhong Wang helped with SEM characterization. F. Benjamin Holness and Aaron D. Price gave some suggestions on the 3D printing technique. Matthew Zheng gave some suggestions for the writing. Ruying Li helped with purchasing chemicals and characterizations. All authors discussed the results and commented on the manuscript.

Notes

The authors declare no competing financial interest.

ACKNOWLEDGMENTS

The work was supported by Natural Science Foundation of China (NSFC) (Grant U1432249), the National Key R&D Program of China (Grant 2017YFA0205002), and the Priority Academic Program Development (PAPD) of Jiangsu Higher Education Institutions. This is also a project supported by Jiangsu Key Laboratory for Carbon-Based Functional Materials and Devices and Collaborative Innovation Center of Suzhou Nano Science & Technology. This work was also supported by the Natural Science and Engineering Research Council of Canada (NSERC), the Canada Research Chair Program (CRC), the Canada Foundation for Innovation (CFI), and the University of Western Ontario (UWO).

REFERENCES

(1) Lu, L.; Han, X.; Li, J.; Hua, J.; Ouyang, M. A Review On The Key Issues For Lithium-Ion Battery Management In Electric Vehicles. *J. Power Sources* **2013**, *226*, 272−288.

(2) Nitta, N.; Wu, F.; Lee, J. T.; Yushin, G. Li-Ion Battery Materials: Present and Future. *Mater. Today* **2015**, *18*, 252−264.

(3) Tarascon, J. M.; Armand, M. Issues and Challenges Facing Rechargeable Lithium Batteries. *Nature* **2001**, *414*, 359−367.

(4) Wang, J.; Sun, X. Olivine $LiFePO_4$: The Remaining Challenges for Future Energy Storage. *Energy Environ. Sci.* **2015**, *8*, 1110−1138.

(5) Gao, X.; Wang, J.; Zhang, D.; Nie, K.; Ma, Y.; Zhong, J.; Sun, X. Hollow $NiFe_2O_4$ Nanospheres on Carbon Nanorods as A Highly Efficient Anode Material for Lithium-Ion Batteries. *J. Mater. Chem. A* **2017**, *5*, 5007−5012.

(6) Li, X.; Gu, M.; Hu, S.; Kennard, R.; Yan, P.; Chen, X.; Wang, C.; Sailor, M. J.; Zhang, J.-G.; Liu, J. Mesoporous Silicon Sponge as An Anti-Pulverization Structure for High-Performance Lithium-Ion Battery Anodes. *Nat. Commun.* **2014**, *5*, 4105−4112.

(7) Gao, X.; Wang, J.; Zhang, D.; Adair, K.; Feng, K.; Sun, N.; Zheng, H.; Shao, H.; Zhong, J.; Ma, Y.; Sun, X.; Sun, X. Carbon Coated Bimetallic Sulfide Nanodots/Carbon Nanorod Heterostructure Enabling Long-Life Lithium-Ion Batteries. *J. Mater. Chem. A* **2017**, *5*, 25625−25631.

(8) Gallagher, K. G.; Trask, S. E.; Bauer, C.; Woehrle, T.; Lux, S. F.; Tschech, M.; Lamp, P.; Polzin, B. J.; Ha, S.; Long, B.; Wu, Q.; Lu, W.; Dees, D. W.; Jansen, A. N. Optimizing Areal Capacities Through Understanding the Limitations of Lithium-Ion Electrodes. *J. Electrochem. Soc.* **2016**, *163*, A138−A149.

(9) Jin, S.; Xin, S.; Wang, L.; Du, Z.; Cao, L.; Chen, J.; Kong, X.; Gong, M.; Lu, J.; Zhu, Y.; Ji, H.; Ruoff, R. S. Covalently Connected Carbon Nanostructures for Current Collectors in Both the Cathode and Anode of Li−S Batteries. *Adv. Mater.* **2016**, *28*, 9094−9102.

(10) Park, J.; Li, J.; Lu, W.; Sastry, A. M. Geometric Consideration of Nanostructures for Energy Storage Systems. *J. Appl. Phys.* **2016**, *119*, 025101.

(11) Chen, C.; Zhang, Y.; Li, Y.; Kuang, Y.; Song, J.; Luo, W.; Wang, Y.; Yao, Y.; Pastel, G.; Xie, J.; Hu, L. Highly Conductive, Lightweight, Low-Tortuosity Carbon Frameworks as Ultrathick 3D Current Collectors. *Adv. Energy Mater.* **2017**, *7*, 1700595.

(12) Lawes, S.; Sun, Q.; Lushington, A.; Xiao, B.; Liu, Y.; Sun, X. Inkjet-Printed Silicon as High Performance Anodes for Li-Ion Batteries. *Nano Energy* **2017**, *36*, 313−321.

(13) Zheng, H.; Li, J.; Song, X.; Liu, G.; Battaglia, V. S. A Comprehensive Understanding of Electrode Thickness Effects on The Electrochemical Performances of Li-Ion Battery Cathodes. *Electrochim. Acta* **2012**, *71*, 258−265.

(14) Jiang, F.; Peng, P. Elucidating the Performance Limitations of Lithium-ion Batteries Due to Species and Charge Transport through Five Characteristic Parameters. *Sci. Rep.* **2016**, *6*, 32639−32657.

(15) Long, J. W.; Dunn, B.; Rolison, D. R.; White, H. S. Three-Dimensional Battery Architectures. *Chem. Rev.* **2004**, *104*, 4463−4492.

(16) Chen, L.; Tang, X.; Xie, P.; Xu, J.; Chen, Z.; Cai, Z.; He, P.; Zhou, H.; Zhang, D.; Fan, T. 3D Printing of Artificial Leaf With Tunable Hierarchical Porosity for CO_2 Photoreduction. *Chem. Mater.* **2018**, *30*, 799−806.

(17) Wei, T.-S.; Ahn, B. Y.; Grotto, J.; Lewis, J. A. 3D Printing of Customized Li-Ion Batteries with Thick Electrodes. *Adv. Mater.* **2018**, *30*, 1703027.

(18) Hu, J.; Jiang, Y.; Cui, S.; Duan, Y.; Liu, T.; Guo, H.; Lin, L.; Lin, Y.; Zheng, J.; Amine, K.; Pan, F. 3D-Printed Cathodes of $LiMn_{1-x}Fe_xPO_4$ Nanocrystals Achieve Both Ultrahigh Rate and High Capacity for Advanced Lithium-Ion Battery. *Adv. Energy Mater.* **2016**, *6*, 1600856.

(19) Jiang, Y.; Xu, Z.; Huang, T.; Liu, Y.; Guo, F.; Xi, J.; Gao, W.; Gao, C. Direct 3D Printing of Ultralight Graphene Oxide Aerogel Microlattices. *Adv. Funct. Mater.* **2018**, *28*, 1707024.

(20) Lawes, S.; Riese, A.; Sun, Q.; Cheng, N.; Sun, X. Printing Nanostructured Carbon for Energy Storage and Conversion Applications. *Carbon* **2015**, *92*, 150−176.

(21) Ladd, C.; So, J.-H.; Muth, J.; Dickey, M. D. 3D Printing of Free Standing Liquid Metal Microstructures. *Adv. Mater.* **2013**, *25*, 5081−5085.

(22) Li, J.; Leu, M. C.; Panat, R.; Park, J. A Hybrid Three-Dimensionally Structured Electrode for Lithium-Ion Batteries via 3D Printing. *Mater. Des.* **2017**, *119*, 417−424.

(23) Choi, K.-H.; Ahn, D. B.; Lee, S.-Y. Current Status and Challenges in Printed Batteries: Toward Form Factor-Free, Monolithic Integrated Power Sources. *ACS Energy Lett.* **2018**, *3*, 220−236.

(24) Sun, K.; Wei, T. S.; Ahn, B. Y.; Seo, J. Y.; Dillon, S. J.; Lewis, J. A. 3D printing of Interdigitated Li-Ion Microbattery Architectures. *Adv. Mater.* **2013**, *25*, 4539−4543.

(25) Fu, K.; Wang, Y.; Yan, C.; Yao, Y.; Chen, Y.; Dai, J.; Lacey, S.; Wang, Y.; Wan, J.; Li, T.; Wang, Z.; Xu, Y.; Hu, L. Graphene Oxide-Based Electrode Inks for 3D-Printed Lithium-Ion Batteries. *Adv. Mater.* **2016**, *28*, 2587−2594.

(26) Ding, J.; Shen, K.; Du, Z.; Li, B.; Yang, S. 3D-Printed Hierarchical Porous Frameworks for Sodium Storage. *ACS Appl. Mater. Interfaces* **2017**, *9*, 41871−41877.

(27) Cho, S.-J.; Choi, K.-H.; Yoo, J.-T.; Kim, J.-H.; Lee, Y.-H.; Chun, S.-J.; Park, S.-B.; Choi, D.-H.; Wu, Q.; Lee, S.-Y.; Lee, S.-Y. Hetero-Nanonet Rechargeable Paper Batteries: Toward Ultrahigh Energy Density and Origami Foldability. *Adv. Funct. Mater.* **2015**, *25*, 6029−6040.

(28) Evanoff, K.; Khan, J.; Balandin, A. A.; Magasinski, A.; Ready, W. J.; Fuller, T. F.; Yushin, G. Towards Ultrathick Battery Electrodes: Aligned Carbon Nanotube-Enabled Architecture. *Adv. Mater.* **2012**, *24*, 533−537.

(29) Liu, C.; Cheng, X.; Li, B.; Chen, Z.; Mi, S.; Lao, C. Fabrication and Characterization of 3D-Printed Highly-Porous 3D $LiFePO_4$ Electrodes by Low Temperature Direct Writing Process. *Materials* **2017**, *10*, 934−947.

(30) Shaijumon, M. M.; Perre, E.; Daffos, B.; Taberna, P. L.; Tarascon, J. M.; Simon, P. Nanoarchitectured 3D Cathodes for Li-Ion Microbatteries. *Adv. Mater.* **2010**, *22*, 4978−4981.

(31) Kohlmeyer, R. R.; Blake, A. J.; Hardin, J. O.; Carmona, E. A.; Carpena-Núñez, J.; Maruyama, B.; Daniel Berrigan, J.; Huang, H.; Durstock, M. F. Composite Batteries: A Simple yet Universal Approach to 3D Printable Lithium-Ion Battery Electrodes. *J. Mater. Chem. A* **2016**, *4*, 16856−16864.

(32) Li, J.; Liang, X.; Liou, F.; Park, J. Macro-/Micro-Controlled 3D Lithium-Ion Batteries via Additive Manufacturing and Electric Field Processing. *Sci. Rep.* **2018**, *8*, 1846−1857.

(33) Gao, L.; Jin, Y.; Liu, X.; Xu, M.; Lai, X.; Shui, J. A Rationally Assembled Graphene Nanoribbon/Graphene Framework for High Volumetric Energy and Power Density Li-Ion Batteries. *Nanoscale* **2018**, *10*, 7676−7684.

(34) Hur, J. I.; Smith, L. C.; Dunn, B. High Areal Energy Density 3D Lithium-Ion Microbatteries. *Joule* **2018**, *2*, 1187−1201.

DOI: 10.1021/acsami.8b14797
ACS Appl. Mater. Interfaces XXXX, XXX, XXX−XXX